Fluorescence recognition of Zn2+ ion by 1,1'-binaphthyl based on polyamine macrocycle

Hiroki Tokunaga
Tokyo Denki University - Tokyo Senju Campus: Tokyo Denki Daigaku - Tokyo Senju Campus
Masaki Tsuboi
Tokyo Denki University - Tokyo Senju Campus: Tokyo Denki Daigaku - Tokyo Senju Campus
Nachika Matsumoto
Tokyo Denki University - Tokyo Senju Campus: Tokyo Denki Daigaku - Tokyo Senju Campus
Makoto Miyasaka (miyasaka@mail.dendai.ac.jp)
Tokyo Denki University https://orcid.org/0000-0001-5527-8307

Research Article

Keywords: BINOL derivative, Macrocycle, Fluorescence

Posted Date: September 13th, 2021

DOI: https://doi.org/10.21203/rs.3.rs-886351/v1

Abstract

Chiral polyimine macrocycles were synthesized by the self-condensation of (*R*)-2,2'-dihydroxy-1,1'-binaphthalene-3,3'-dicarbaldehyde and *o*-phenylenediamine derivatives under template-free conditions in relatively high yields, and the corresponding polyamine macrocycles were obtained by the reduction of the polyimine macrocycles. The complexation behaviors of the polyamine macrocycles with different metal cations in ethanol were studied based on their UV-vis absorption spectra and fluorescence spectra. No fluorescence was observed for the polyimine macrocycles (*R,R*)-**1**–(*R,R*)-**3**, however, (*R,R*)-**1H** and (*R,R*)-**2H** exhibited a “turn-on” blue fluorescence (λ_{em} = 415 nm) that were observed upon the addition of Zn^{2+}. Especially, (*R,R*)-**3H** complexed with Zn^{2+} also produced a “turn-on” yellowish green fluorescence (λ_{em} = 510 nm).

1. Introduction

Shape-persistent chiral macrocycles [1–3] have been studied for their applications in molecular recognition, supramolecular architectures, and use as an asymmetric catalyst [4–6] and a novel fluorescence responsive probe (chemosensor) [7–10].

Especially, the axially chiral 1,1'-binaphthyl skeleton has been widely investigated in the field of asymmetric catalysis, molecular recognition, and optically-active molecules including polymers for the past several decades [11–14]. The advantage of using the 1,1'-binaphthyl structure is that numerous methods have been developed to selectively functionalize on the 1,1'-bi-2-naphthol (BINOL), which lead to the design and synthesis of structurally unique derivatives. Novel macrocyclic Schiff base structures based on 1,1'-binaphthyl and their application such as fluorescent chemosensors or colorimetric molecular probes are of the great interest [15–17].

Brunner *et al.*, reported the synthesis of the chiral bisbinaphthyl macrocycles (**I** in Chart 1) [18] and Pu *et al.* then reported the enantioselective fluorescent recognition for a-hydroxycarboxylic acids using **I** [19]. Also, Pu *et al.* investigated that discrimination such as amino alcohols and amino acids using polyimine macrocycles reduced from **I** was done [20]. Cheng *et al.* also investigated the turn-on and turn-off fluorescent chemosensor for the Zn^{2+} ion and Cu^{2+} ion, respectively using the macrocycle derivatives (**II** in Chart 1) [21, 22]. Recently, Pu *et al.* revisited the 1,1'-binaphthyl-based macrocycle and described a unique response against the Hg^{2+} ion [23]. While there is a lot of research about fluorescent chemosensor using acyclic Schiff base compounds [24–28], there is a limited number of Schiff base macrocycles [29–36].

Insert Chart 1 here

However, there is only one report using an achiral diamine, such as phenylenediamine (**III** in Chart 1) [37], and the obtained chiral macrocycle showed an excellent chiroptical properties. However, there has been no detailed investigation about the fluorescent response toward a variety of metal cations using this macrocycle. Herein, we have reported the synthesis of conjugated and non-conjugated macrocycles

consisting of bisbinaphthyl and *o*-phenylenediamine derivatives and examined the fluorescent behavior of these macrocycles under the addition of the metal cations.

2. Experimental Section

2.1. *Materials*

All the reagents were purchased from commercial suppliers (Wako Chemical) and used without any further purification.

2.2. *Measurements*

The ^{1}H NMR and ^{13}C NMR spectra were measured by a Bruker DPX-300 MHz spectrometer using chloroform-*d*, DMSO-d_6, and acetone- d_6 as the solvents. The FT-IR spectra were obtained using a JEOL JIR-WINSPEC50 (32 scans, 4000–400 cm^{-1}, 4 cm^{-1} resolution). The UV-vis spectra were recorded by a SHIMADZU (UV-2600) spectrophotometer. The fluorescence spectra were obtained by a JASCO FP-6500 spectrometer with the excitation and emission slit widths of both 3.0 nm. The optical rotations were measured by a POLAX-2L (Atago Co., Ltd.) at ambient temperature.

2.3. *Synthesis of conjugated macrocycles* (***R,R***)-**1**–(***R,R***)-**3**.

A typical procedure for the synthesis of the conjugated macrocyclic polyimine (***R,R***)-**1** was as follows: The diformyl derivative **1** [37] (1.0038 g, 2.93 mmol) and *o*-phenylenediamine (**2**, 0.3174 g, 2.94 mmol) were stirred in 128 mL of DMF at 80 °C for 24 h. The usual aqueous workup with hexane/ethyl acetate gave the crude product as an orange solid. Treatment of the crude product with methanol gave the product as a yellow solid after filtration.

(***R,R***)-**1**: Yield 81%. m.p. > 300 °C. ^{1}H-NMR (300 MHz, $CDCl_3$, TMS, Figure 1S in the Supporting Information) δ (ppm) = 12.53 (s, 4H, OH), 8.76 (s, 4H, CH=N), 8.03 (s, 4H), 7.84–7.78 (m, 4H), 7.38–7.32 (m, 4H), 7.24–7.10 (m, 16H). FT-IR (KBr, cm^{-1}): 3056 (ν_{O-H}), 1616 ($\nu_{C=N}$). [α]D = −1692° (*c* = 0.065, $CHCl_3$). UV-vis ($CHCl_3$) λmax (ε) = 266 (1.0×10^5), 314 (7.2×10^4), 370 (3.5×10^4).

(***R,R***)-**2**: Yield 93%. m.p. > 300 °C. ^{1}H-NMR (300 MHz, $CDCl_3$, TMS, Figure 3S in the Supporting Information) δ (ppm) = 12.65 (s, 1H, OH), 12.61 (s, 1H, OH), 12.58 (s, 1H, OH), 12.54 (s, 1H, OH), 8.74 (s, 2H, CH=N), 8.73 (s, 2H, CH=N), 8.01 (s, 4H), 8.05–7.95 (m, 4H), 7.85–7.75 (m, 4H), 7.20–7.08 (m, 10H), 7.02–6.98 (m, 2H), 6.91–6.89 (m, 2H), 2.42 (s, 6H, CH_3). FT-IR (KBr, cm^{-1}): 3055 (ν_{O-H}), 1616 ($\nu_{C=N}$). [α]D = −1604° (*c* = 0.235, $CHCl_3$). UV-vis ($CHCl_3$) λmax (ε) = 268 (1.1×10^5), 314 (7.0×10^4), 372 (3.8×10^4).

(***R,R***)-**3**: Yield 95%. m.p. > 300 °C. ^{1}H-NMR (300 MHz, $CDCl_3$, TMS, Figure 5S in the Supporting Information) δ (ppm) = 12.33 (s, 1H, OH), 12.31 (s, 1H, OH), 12.23 (s, 1H, OH), 12.21 (s, 1H, OH), 8.75–8.70 (m, 4H, CH=N), 8.06–8.01 (m, 4H), 7.83–7.78 (m, 4H), 7.46 (dd, *J* = 2.0 Hz, 8.3 Hz, 2H), 7.28–7.20 (m,

10H), 7.18–7.10 (m, 4H), 6.97 (dd, *J* = 1.8 Hz, 8.4 Hz, 2H). FT-IR (KBr, cm^{-1}): 3055 (ν_{O-H}), 1616 ($\nu_{C=N}$). [α]D = −1550° (*c* = 0.235, $CHCl_3$). UV-vis ($CHCl_3$) λmax (ε) = 268 (1.0×10^5), 316 (7.7×10^4), 370 (4.0×10^4).

2.4. *Synthesis of non-conjugated macrocycles* (***R,R***)-**1H–**(***R,R***)-**3H**.

A typical procedure for the synthesis of the non-conjugated macrocycle was as follows: A mixture of (***R,R***)**-1** (0.4207 g, 508 mmol) and $NaBH_4$ (powder (after ground) 0.114 g, 3.0 mmol, 6 equiv) in ethanol (80 mL) was refluxed for 4 h. The mixture was cooled to RT with stirring for another 2 h after the addition of ca. 1% HCl (62 mL) and $CHCl_3$ (62 mL). The reaction mixture was neutralized with $NaHCO_3$ aq., extracted with chloroform, washed with water, dried over Na_2SO_4, and evaporated to give the crude product as an orange solid. The crude product was purified by short column chromatography on silica with chloroform/methanol (= 100:1) eluent to give the product as a pale-yellow solid (0.2542 g, 60%).

(***R,R***)-**1H**: Yield 60%. ^{1}H-NMR (300 MHz, $CDCl_3$, TMS, Figure 2S in the Supporting Information) δ (ppm) = 7.80–7.74 (m, 8H), 7.28 (td, *J* = 1.6 Hz, 9.4 Hz, 4H), 7.18 (td, *J* = 1.7 Hz, 9.7 Hz, 4H), 7.02 (d, *J* = 8.4 Hz, 4H), 6.99–6.92 (m, 8H), 4.50–4.36 (m, 8H), 1.71 (br s, 4H, NH). FT-IR (KBr, cm^{-1}): 3629, 3512 (ν_{N-H}), 3292 (ν_{O-H}). [α]D = +171° (*c* = 0.105, $CHCl_3$). UV-vis (EtOH) λmax (ε) = 242 (1.5×10^5), 282 (4.1×10^4), 324 (2.6×10^4), 334 (2.8×10^4), 384 (3.8×10^4).

(***R,R***)-**2H**: Yield 93%. ^{1}H-NMR (300 MHz, $CDCl_3$, TMS, Figure 4S in the Supporting Information) δ (ppm) = 12.64–12.54 (m, 4H), 8.74–8.73 (m, 4H), 8.00 (s, 4H), 7.81–7.78 (m, 4H), 7.23–7.19 (m, 8H), 7.15–7.12 (m, 6H), 7.01–6.99 (m, 4H), 6.85 (s, 4H), 2.42 (s, 6H). [α]D = +170° (*c* = 0.182, $CHCl_3$). UV-vis ($CHCl_3$) λ_{max} (ε) = 266 (1.1×10^5). UV-vis (EtOH) λmax (ε) = 230 (3.3×10^5), 334 (4.1×10^4).

(***R,R***)-**3H**: Yield 91%. ^{1}H-NMR (300 MHz, $CDCl_3$, TMS, Figure 6S in the Supporting Information) δ (ppm) = 7.85–7.70 (m, 8H), 7.40–7.15 (m, 8H), 7.10–6.90 (m, 8H), 6.77 (d, *J* = 8.3 Hz, 2H), 4.45–4.25 (m, 8H, CH_2). FT-IR (KBr, cm^{-1}): 3629, 3510 (ν_{N-H}), 3302 (ν_{O-H}). [α]D = +165° (*c* = 0.224, $CHCl_3$). UV-vis (EtOH) λ_{max} (ε) = 230 (3.8×10^5), 338 (3.1×10^4).

3. Results And Discussion

The [2+2] polyimine macrocycles (*R,R*)-**1–**(*R,R*)-**3** were selectively obtained by Schiff base formation between the optically-active binaphthyl derivatives: (*R*)-3,3'-dialdehyde-BINOL (**1**) [35, 36] and achiral *o*-phenylenediamine derivatives in DMF at 80 °C in good yields (80~90%, Scheme 1). The advantages of these compounds are being obtained in high yield only by the addition of the crude reaction mixture into methanol. The metal complexation of the chiral conjugated macrocycle obtained with various metal ions was examined. A change in the absorption spectrum was observed after the addition of Co^{2+}, Ni^{2+}, Cu^{2+}, Zn^{2+}, and Pd^{2+} other than Hg^{2+}. However, no significant change in fluorescence spectra was observed for (*R,R*)-**1–**(*R,R*)-**3**. Therefore, the non-conjugated macrocycles were obtained through the $NaBH_4$ reduction of (*R,R*)-**1H–**(*R,R*)-**3H** in moderate yields (~60%, Scheme 2).

Insert Scheme 1 here

The chiral nature of the obtained polyimine macrocycles were evaluated by the specific optical rotation $[\alpha]_D$. [α]D values of (*R,R*)-**1**–(*R,R*)-**3** that are *ca*. 6 fold higher accompanied with a change in the sign after the formation of the cyclic structure compared to the precursor (*R*)-**1**. On the other hand, the [α]D dramatically decreased after reduction of the imine and the sign of [α]D of (*R,R*)-**1H**–(*R,R*)-**3H** showed the same sign as **1**.

The UV-vis and fluorescence spectra of (*R,R*)-**1H** at various concentrations in ethanol were examined. Plots of the absorbance intensity versus the concentration of (*R,R*)-**1H** show that the linear relationship up to the concentration of 2.5×10^{-5} M indicated that (*R,R*)-**1H** does not form ground state intermolecular aggregates. However, the fluorescence intensity at 495 nm versus the concentration of (*R,R*)-**1H** show that the deviation at a concentration greater than 2.0×10^{-5} M (Figure 1(a)). The absorption and fluorescence spectra of (*R,R*)-**2H** (Figure 7S in the Supporting Information) and (*R,R*)-**3H** (Figure 1(b)) show a tendency similar to (*R,R*)-**1H** (Figure 1(a)). For example, (*R,R*)-**1H**–(*R,R*)-**3H** emits at almost similar fluorescence wavelengths, which are 495 nm, 485 nm, and 495 nm, respectively. No significant substitution effects were observed.

Insert Figure 1 here

(*R,R*)-**1H** in ethanol solution was treated with 2 equiv. of various metal cations and both the absorption and fluorescence response were recorded. An absorption spectrum change was observed after the addition of the metal cations such as Co^{2+}, Ni^{2+}, Cu^{2+}, Zn^{2+}, and Hg^{2+}. Also, the fluorescence spectra of (*R,R*)-**1H** with Co^{2+}, Ni^{2+}, Cu^{2+}, and Hg^{2+} ions weakened the emission intensity, while only the Zn^{2+} ion leads to a pronounced fluorescence enhancement at 405 nm (Figure 2(a)). By applying a commercially-available UV lamp (l_{max} = 365 nm), significant color changes (blue emission) were observed upon the addition of Zn^{2+} over the other metal ions (Figure 2(b)). In the case of (*R,R*)-**2H**, the absorption and emission behavior was similar to (*R,R*)-**1H** after complexation of the metal ions. However, (*R,R*)-**3H** also shows quenching by the addition of Co^{2+}, Ni^{2+} and Cu^{2+}, and in the case of Zn^{2+} and Hg^{2+}, the emission intensity decreased, but the ratio of the decrease was small for Zn^{2+}, indicating a yellowish green fluorescence. The reason for the fluorescence enhancement after Zn^{2+} addition to receptor (*R,R*)-**1H**–(*R,R*)-**3H** is based on the inhibition of photo-induced-electron-transfer (PET) process. The lone pair of electrons on the nitrogen atom cannot contribute to PET process, electron attracting ability is lower than other metal ions (Co^{2+}, Ni^{2+} and Cu^{2+}), which provide the fluorescence enhancement [9, 10, 21, 38].

Insert Figure 2 here

The absorption spectral variation of (*R,R*)-**1H** upon the gradual addition of Zn^{2+} ions is shown in Figure 3. The absorption spectrum of (*R,R*)-**1H** itself exhibits 230 nm and 334 nm in ethanol. Upon the gradual addition of Zn^{2+}, the absorbance at 230 nm gradually decreased, and concomitantly, the new absorption bands at 246 nm and 350 nm gradually increased. Two isosbestic points at 240 nm and 334 nm were

observed. Besides, the newly observed absorbance at 350 nm finally reached a plateau after 2.0 equiv amounts of Zn^{2+} were added (Inset in Figure 3).

Insert Figure 3 here

The Job's plot (Figure 4) showed a maximum mole fraction of (*R,R*)-**1H** about 0.3 at 405 nm. This clearly indicated a 1:2 (*R,R*)-**1H**–Zn^{2+} stoichiometry.

Insert Figure 4 here

The association for the (*R,R*)-**1H**–Zn^{2+} stoichiometry was also confirmed by the Benesi–Hildebrand analysis (Figure 5) [39–41].

$$\frac{1}{F-F_0}=\frac{1}{K(F_{max}-F_0)[Zn^{2+}]^n}+\frac{1}{F_{max}-F_0} \qquad (1)$$

F_0 is the emission intensity of (*R,R*)-**1H** without metal ions. *F* is the emission intensity in the presence of Zn^{2+}, F_{max} is the emission intensity obtained with an excess amount of Zn^{2+}, $[Zn^{2+}]$ is the concentration of Zn^{2+}, and *K* is the association constant between (*R,R*)-**1H** and Zn^{2+}. Based on the plot of $1/(F-F_0)$ versus $1/[Zn^{2+}]^2$, it shows a linear relationship, indicating that (*R,R*)-**1H** associates with Zn^{2+} in a 1:2 stoichiometry. The association constant, *K*, between (*R,R*)-**1H** and the two Zn^{2+} ions, was estimated to be 4.4×10^9 M^{-2}. The observed high *K* value clearly indicated the strong affinity of Zn^{2+} toward (*R,R*)-**1H**.

Insert Figure 5 here

^{1}H-NMR titration experiments were carried out in DMSO-d_6 in order to gain further information about the coordination behavior under the addition of Zn^{2+}. The signal shifts in spectrum were observed until the addition of 2.0 equiv Zn^{2+} as shown in Figure 6. A hydroxyl signal at 8.68 ppm disappeared with a weak broad peak appearance around 12 ppm, which could be attributed to the hydroxyl group. Also, the broad peak could be assigned to the amino group around and 6.1 and 4.7 ppm could be downfield shifted and observed. Additionally, the signals of the aromatic and aliphatic ($-CH_2-$) are broader than those in the absence of Zn^{2+}. No change was observed after the further addition of Zn^{2+}, indicating the coordination of the additional Zn^{2+} to form the 1:2 complex. Also, the binol hydroxyl groups in (*R,R*)-**1H** were involved in the coordination of the Zn^{2+} ions accompanied with the amino group. Based on these spectral results, a 1:2 complex of (*R,R*)**-1H** and Zn^{2+} was proposed as depicted in Figure 6.

Insert Figure 6 here

To prove how the diamine unit moiety affects the emissions of the complex, (*R,R*)-**1H–**(*R,R*)-**3H** was chosen to discuss. (*R,R*)-**1H**–(*R,R*)-**3H** emits almost similar fluorescence wavelength which were 495 nm, 485 nm, and 495 nm. On the other hand, as shown in Figure 7, the fluorescence emissions of the complex

of (*R,R*)-**1H**–(*R,R*)-**3H** with Zn^{2+} appeared at 405 nm, 415 nm, and 510 nm. The bromide-substituted non-conjugated macrocycle (*R,R*)-**3H** emission dramatically changed to a longer wavelength, which implied the substituent effect was clearly observed.

In the fluorescence measurement of (*R,R*)-**1H**–(*R,R*)-**3H**, a decrease in the fluorescence intensity was observed at concentrations of more than 20 μM. In the case of (*R,R*)-**1H** and (*R,R*)-**2H** after the addition of zinc, the linearity of the relationship between the intensity and the concentration was maintained up to 50 μM and 30 μM, respectively. However, in the case of (*R,R*)-**3H**, no decrease in the fluorescence intensity was confirmed in the measured concentration range and it showed a good linearity. Furthermore, the emission of the zinc complex of (*R,R*)-**3H** was yellowish green, (*R,R*)-**2H**, while the zinc complex of (*R,R*)-**2H** is blue, which is easy to distinguish.

Insert Figure 7 here

4. Conclusions

We obtained three conjugated macrocycles by the [2+2] self-condensation of diformyl bisbinaphthyl and 1,2-diaminobenzene derivatives, and the reduction of the obtained conjugated macrocycles using $NaBH_4$ which lead to the corresponding non-conjugated macrocycles were achieved. The fluorescent behavior of (*R,R*)-**1H–**(*R,R*)-**3H** itself in ethanol with no-substituent or substitution with a electron donating (methyl) group or electron accepting group (bromo group) show almost similar fluorescences. However, the fluorescent behavior of these macrocycles upon the addition of Zn^{2+} showed a “turn-on” response with the different emission wavelengths. (*R,R*)-**1H** and (*R,R*)-**2H** complexed with Zn^{2+} exhibited blue emission, on contrary, the bromo-substituted (*R,R*)-**3H** complexed with Zn^{2+} also detected “turn-on” yellowish green fluorescence (λ_{em} = 510 nm). Although (*R,R*)-**1H–**(*R,R*)-**3H** is the simple [2+2] polyamine macrocycle structure, development of extended shape-persistent macrocycles based on BINOL framework may contribute to the and more efficient and more useful chemosensors. Furthermore, we are currently investigating the novel chiroptical property such as the circular polarized luminescence (CPL) using these metal complexes

Declarations

Funding: Not applicable

Competing interests: The authors declare that they have no competing interests.

Ethics approval/declarations: Not applicable

Consent to participate: Not applicable

Consent for publication: Not applicable

Data availability: The data used to support the conclusions of this article are included within the article and its additional supporting information file.

Code availability Not applicable

Contributions: All authors (Hiroki Tokunaga, Masaki Tsuboi, Nachika Matsumoto) have synthesized and characterized the compounds and contributed to the spectroscopic measurements. Makoto Miyasaka provided the idea, supervised the project, and prepared the manuscript. All authors have given approval to the final version of the manuscript.

References

1. Zhang W, Moore JS (2006) Shape-Persistent Macrocycles: Structures and Synthetic Approaches from Arylene and Ethynylene Building Blocks. Angew Chem Int Ed 45:4416–4439. https://doi.org/10.1002/anie.200503988
2. Hoger S (2004) Shape-Persistent Macrocycles: From Molecules to Materials. Chem Eur J 10:1320–1329. https://doi.org/10.1002/chem.200305496
3. Jiang J, Dong RY, MacLachlan MJ (2015) Lyotropic liquid crystallinity in mixed-tautomer Schiff-base macrocycles. Chem Commun 51:16205–16208. https://doi.org/10.1039/C5CC06253E
4. Gospodarowicz K, Hołyńska M, Paluch M, Lisowski J (2012) Novel chiral hexaazamacrocycles for the enantiodiscrimination of carboxylic acids. Tetrahedron 68:9930–9935. https://doi.org/10.1016/j.tet.2012.09.093
5. Akine S, Utsuno F, Piao S, Orita H, Tsuzuki S, Nabeshima T (2016) Synthesis, Ion Recognition Ability, and Metal-Assisted Aggregation Behavior of Dinuclear Metallohosts Having a Bis(Saloph) Macrocyclic Ligand. Inorg Chem 55:810–821. https://doi.org/10.1021/acs.inorgchem.5b02288
6. Berrones-Reyes JC, Vidyasagar CC, Muñoz Flores BM, Jiménez-Pérez V (2018) Luminescent molecules of main group elements: Recent advances on synthesis, properties and their application on fluorescent bioimaging (FBI). J Lumin 195:290–313. https://doi.org/10.1016/j.jlumin.2017.11.042
7. Liu Y, Zhang Q, Jin W-H, Xu T-Y, Qu D-H, Tian H (2018) Bistable [2]rotaxane encoding an orthogonally tunable fluorescent molecular system including white-light emission. Chem Commun 54:10642–10645. DOI https://doi.org/10.1039/C8CC05886E
8. Li Z-B, Liu T-D, Pu L (2007) Chiral Macrocycle-Catalyzed Highly Enantioselective Phenylacetylene Addition to Aliphatic and Vinyl Aldehydes. J Org Chem 72:4340–4343. https://doi.org/10.1021/jo070091j
9. Bera MK, Chakraborty C, Malik S (2015) How the stereochemistry decides the selectivity: an approach towards metal ion detection. New J Chem 39:9207–9214. https://doi.org/10.1039/C5NJ01148E

10. Bera MK, Chakraborty C, Malik S (2016) Salen-based enantiomeric polymers for enantioselective recognition. New J Chem 40:8074–8080. https://doi.org/10.1039/C6NJ00844E
11. Pu L (2004) Fluorescence of Organic Molecules in Chiral Recognition. Chem Rev 104:1687–1716. https://doi.org/10.1021/cr030052h
12. Shockravi A, Javadi A, Abouzari-Lotf E (2013) Binaphthyl-based macromolecules: a review. RSC Adv 3:6717–6746. https://doi.org/10.1039/C3RA22418J
13. Yu S, Pu L (2015) Recent progress on using BINOLs in enantioselective molecular recognition. Tetrahedron 71:745–772. https://doi.org/10.1016/j.tet.2014.11.007
14. Sunoj RB (2016) Transition State Models for Understanding the Origin of Chiral Induction in Asymmetric Catalysis. Acc Chem Res 49:1019–1028. https://doi.org/10.1021/acs.accounts.6b00053
15. Srimurugan S, Suresh P, Babu B, Pati HN (2008) Chiral Macrocyclic Schiff Bases: An Overview. Mini-Review in Organic Chemistry 5:228–242. 10.2174/157019308785161657
16. MacLachlan MJ (2006) Conjugated shape-persistent macrocycles via Schiff-base condensation: New motifs for supramolecular chemistry. Pure Appl Chem 78:873–888. http://dx.doi.org/10.1351/pac200678040873
17. Pu L (2017) Simultaneous Determination of Concentration and Enantiomeric Composition in Fluorescent Sensing. Acc Chem Res 50:1032–1040. https://doi.org/10.1021/acs.accounts.7b00036
18. Brunner H, Schiessling H (1994) Dialdehyde + Diamine—Polymer or Macrocycle? Angew. Chem Int Ed 33:125–126. https://doi.org/10.1002/anie.199401251
19. Lin J, Zhang H-C, Pu L (2002) Bisbinaphthyl Macrocycle-Based Highly Enantioselective Fluorescent Sensors for α-Hydroxycarboxylic Acids. Org Lett 4:3297–3300. https://doi.org/10.1021/ol026565c
20. Li Z-B, Lin J, Sabat M, Hyacinth M, Pu L (2007) Enantioselective Fluorescent Recognition of Chiral Acids by Cyclohexane-1,2-diamine-Based Bisbinaphthyl Molecules. J Org Chem 72:4905–4916. https://doi.org/10.1021/jo0704715
21. Shen K, Yang X, Cheng Y, Zhu C (2012) A highly selective ratiometric fluorescent chemosensor for Zn^{2+} ion based on a polyimine macrocycle. Tetrahedron 68:5719–5723. https://doi.org/10.1016/j.tet.2012.05.045
22. Yang X, Liu X, Shen K, Zhu C, Cheng Y (2011) A Chiral Perazamacrocyclic Fluorescent Sensor for Cascade Recognition of Cu(II) and the Unmodified α-Amino Acids in Protic Solutions. Org Lett 13:3510–3513. https://doi.org/10.1021/ol2013268
23. Xu X, Trindle CO, Zhang G, Pu L (2015) Fluorescent recognition of Hg^{2+} by a 1,1'-binaphthyl-based macrocycle: a highly selective off–on–off response. Chem Commun 51:8469–8472. https://doi.org/10.1039/C5CC02457A
24. Velmurugan K, Nandhakumar R (2015) Binol based “turn on” fluorescent chemosensor for mercury ion. J Lumin 162:8–13. https://doi.org/10.1016/j.jlumin.2015.01.039

25. Zhangm K, Wu S, Qu D, Wang L (2016) ESIPT-based ratiometric probe for Zn2 + detection based on BINOL framework. Tetrahedron Lett 57:1133–1137. https://doi.org/10.1016/j.tetlet.2016.01.101
26. Munusamy S, Iyer SK (2016) A chiral (S)-BINOL based fluorescent sensor for the recognition of Fe(III) and cascade discrimination of α-amino acids. Tetrahedron: Asymmetry 27 (2016) 492–497. https://doi.org/10.1016/j.tetasy.2016.05.002
27. Roy A, Dey S, Halder S, Roy P (2017) Development of a new chemosensor for Al^{3+} ion: Tuning of properties. J Lumin 192:504–512. https://doi.org/10.1016/j.jlumin.2017.07.020
28. Halder S, Hazra A, Roy P (2018) Colorimetric and fluorescence sensing of pH with a Schiff-base molecule. J Lumin 195:326–333. https://doi.org/10.1016/j.jlumin.2017.11.055
29. Gallant AJ, MacLachlan MJ (2003) Ion-Induced Tubular Assembly of Conjugated Schiff-Base Macrocycles. Angew Chem Int Ed 42:307–5310. https://doi.org/10.1002/anie.200352395
30. Gallant AJ, Patrick BO, MacLachlan MJ (2004) Mild and Selective Reduction of Imines: Formation of an Unsymmetrical Macrocycle. J Org Chem 69:8739–8744. https://doi.org/10.1021/jo049197u
31. Ma C, Lo A, Abdolmaleki A, MacLachlan MJ (2004) Synthesis and Metalation of Novel Fluorescent Conjugated Macrocycles. Org Lett 6:3841–3844. https://doi.org/10.1021/ol0483549
32. Shopsowitz KE, Edwards D, Gallant AJ, MacLachlan MJ (2009) Highly substituted Schiff base macrocycles via hexasubstituted benzene: a convenient double Duff formylation of catechol derivatives. Tetrahedron 65:8113–8119. https://doi.org/10.1016/j.tet.2009.07.094
33. Guieu S, Crane AK, MacLachlan MJ (2011) Campestarenes: novel shape-persistent Schiff basemacrocycles with 5-fold symmetry. Chem Commun 47:1169–1171. https://doi.org/10.1039/C0CC04493H
34. Jiang J, Dong RY, MacLachlan MJ (2015) Lyotropic liquid crystallinity in mixed-tautomer Schiff-base macrocycles. Chem Commun 51:16205–16208. https://doi.org/10.1039/C5CC06253E
35. Li Z-B, Pu L (2004) BINOL – Salen-Catalyzed Highly Enantioselective Alkyne Additions to Aromatic Aldehydes. Org Lett 6:1065–1068. https://doi.org/10.1021/ol0498139
36. Chen C, Huang Q, Zou S, Wang L, Luan B, Zhu J, Wang Q, Pu L (2014) Asymmetric alkyne addition to aldehydes catalyzed by Schiff bases made from 1,1'-bi-2-naphthol and chiral benzylic amines. Tetrahedron: Asymmetry 25:199–201. https://doi.org/10.1016/j.tetasy.2013.12.013
37. Zhang H-C, Huang W-S, Pu L (2001) Biaryl-Based Macrocyclic and Polymeric Chiral (Salophen)Ni(II) Complexes: Synthesis and Spectroscopic Study. J Org Chem 66:481–487. https://doi.org/10.1021/jo001276s
38. Dong W-K, Akogun SF, Zhang Y, Sun Y-X, Dong X-Y (2017) A reversible “turn-on” fluorescent sensor for selective detection of Zn^{2+}. Sens. Actuators B 238:723–734. https://doi.org/10.1016/j.snb.2016.07.047
39. Benesi HA, Hildebrand JH (1949) A Spectrophotometric Investigation of the Interaction of Iodine with Aromatic Hydrocarbons. J Am Chem Soc 71:2703–2707. https://doi.org/10.1021/ja01176a030

40. Shiraishi Y, Sumiya S, Kohno Y, Hirai T (2008) A Rhodamine – Cyclen Conjugate as a Highly Sensitive and Selective Fluorescent Chemosensor for Hg(II). J Org Chem 73:8571–8574. https://doi.org/10.1021/jo8012447
41. Shiraishi Y, Itoh M, Hirai T (2011) Colorimetric response of spiropyran derivative for anions in aqueous or organic media. Tetrahedron 67:891–897. https://doi.org/10.1016/j.tet.2010.12.021

Note

Scheme 1 and Chart 1 are available in the Supplementary Files section

Figures

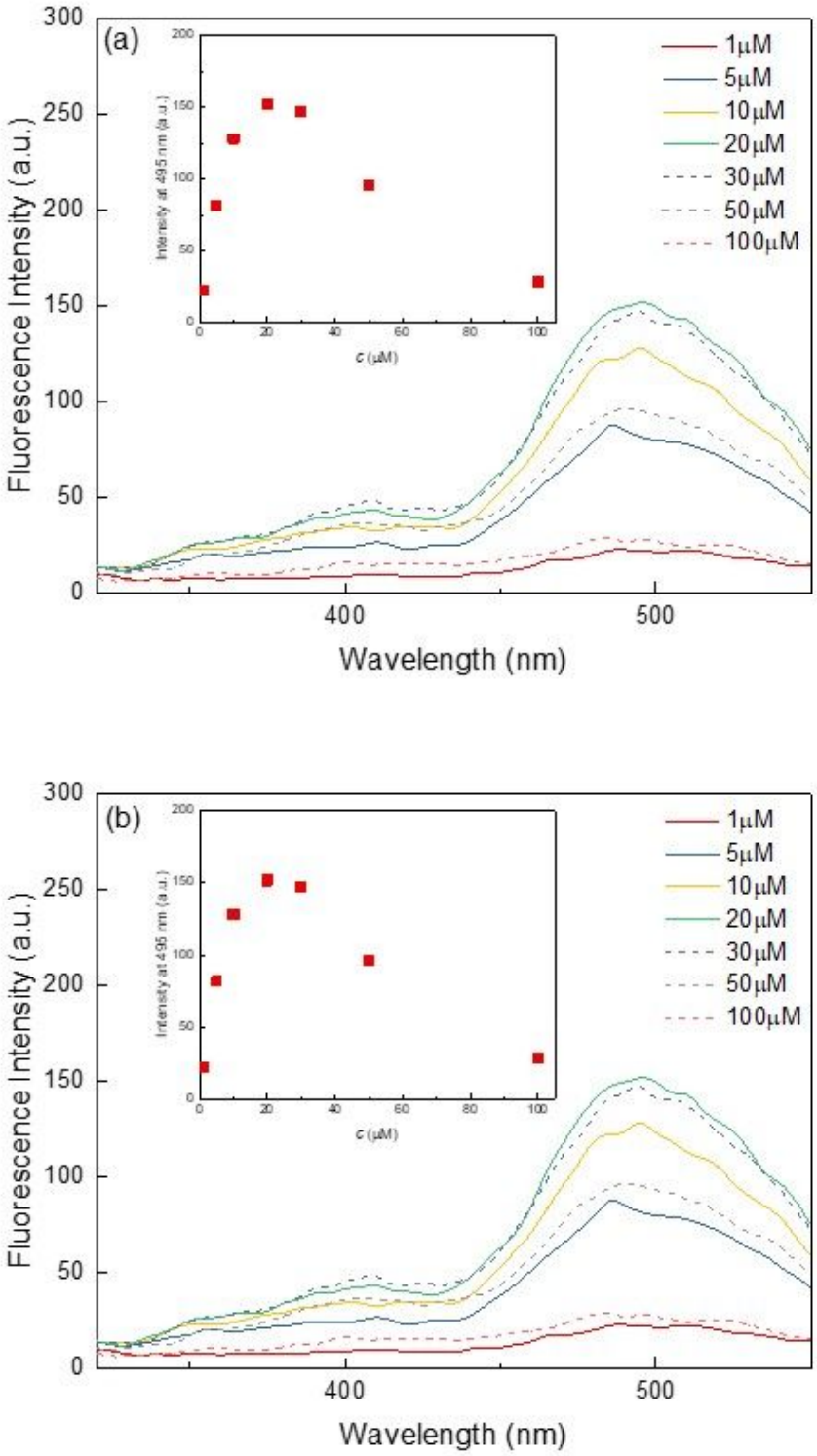

Figure 1

Fluorescence spectra (a) (R,R)-1H and (b) (R,R)-3H at various concentrations in ethanol solution. Inset: the relationship between concentration ([C]) of macrocycle and fluorescence intensity at 495 nm.

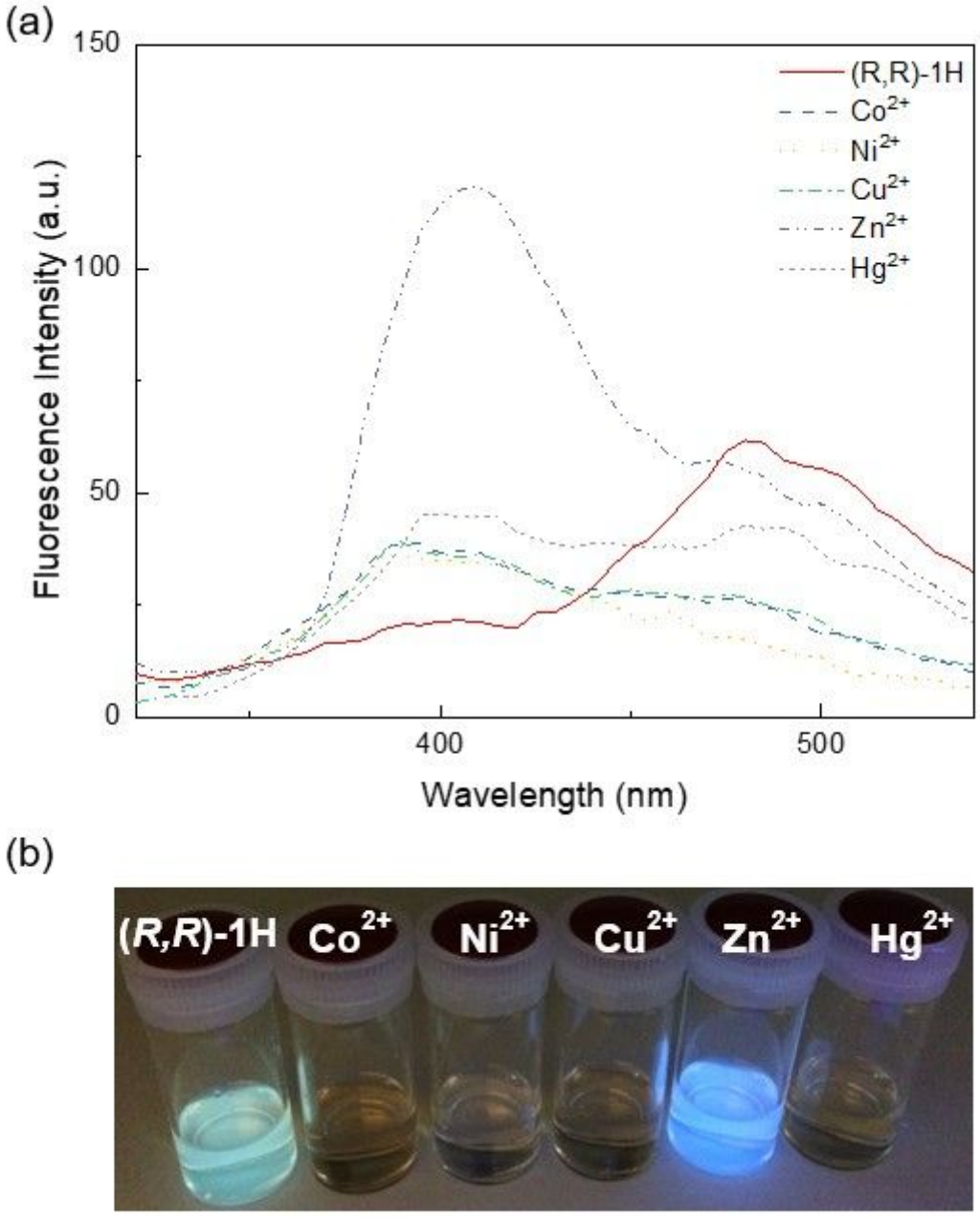

Figure 2

(a) Fluorescence spectra of (R,R)-1H (10 μM, λex = 290 nm) in the absence and presence of 2.0 equiv of various metal ions in EtOH. (b) Fluorescence photographs of a solution of (R,R)-1H in the absence and presence of 2.0 equiv of various metal ions excited by a commercially-available UV lamp (λex = 365 nm).

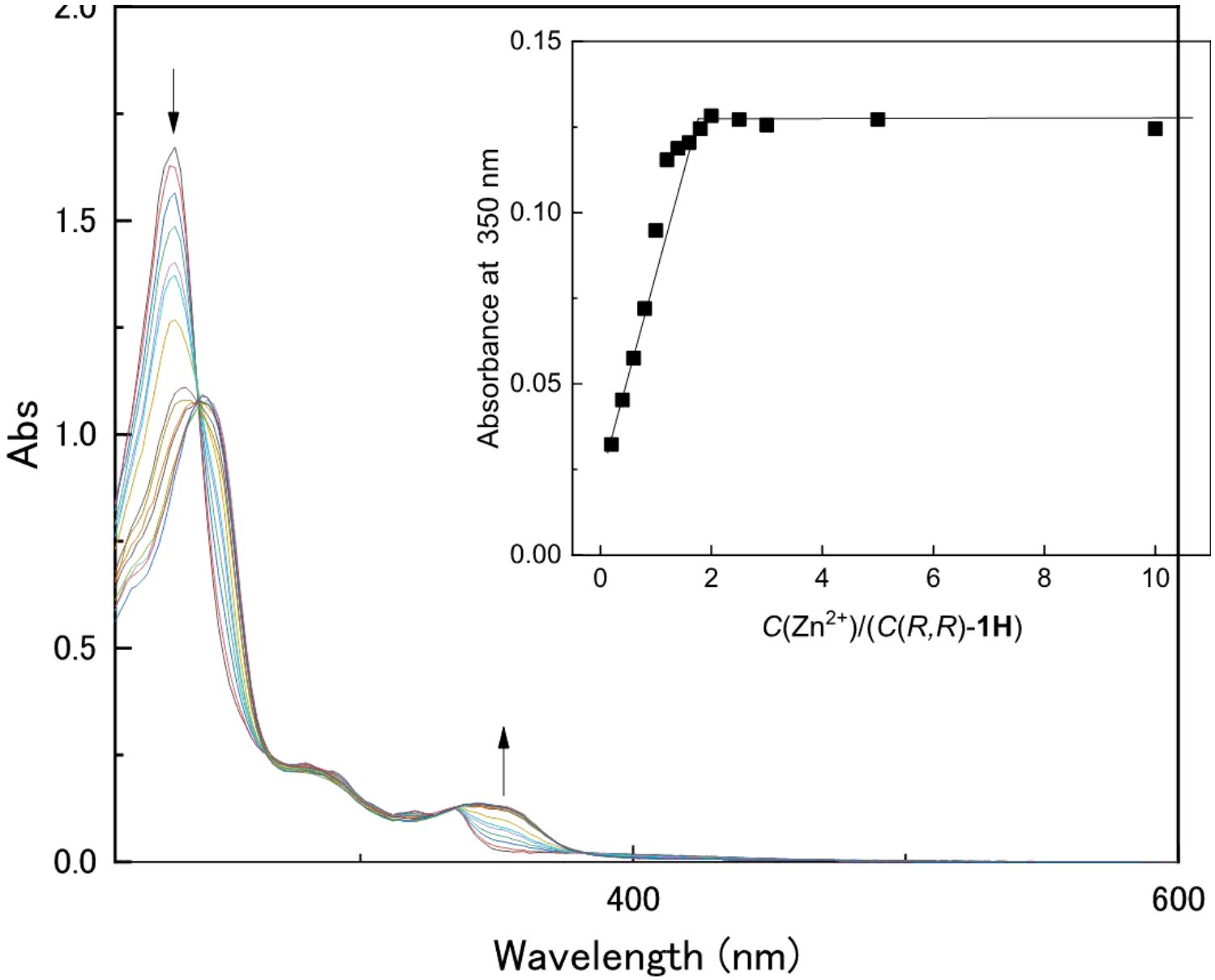

Figure 3

Changes in UV-vis spectra of (R,R)-1H upon the addition of Zn2+ ion (0, 0.2, 0.4, 0.6, 0.8, 1.0, 1.2, 1.4, 1.6, 1.8, 2.0, 2.5, 3.0, 5.0, and 10 equiv Zn2+). Inset: plots of absorbance at 350 nm versus value of C(Zn2+)/C((R,R)-1H), C((R,R)-1H) = 10 μM.

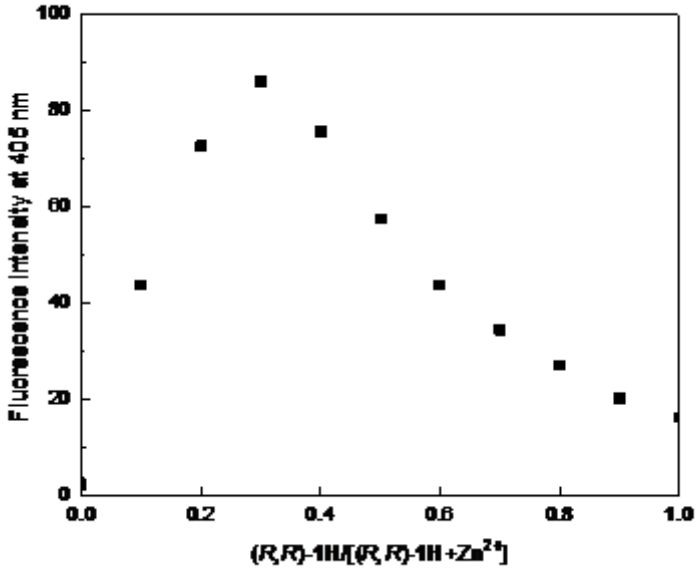

Figure 4

Job's plot for absorption intensity response of complexation of (R,R)-1H with Zn2+ at 354 nm.

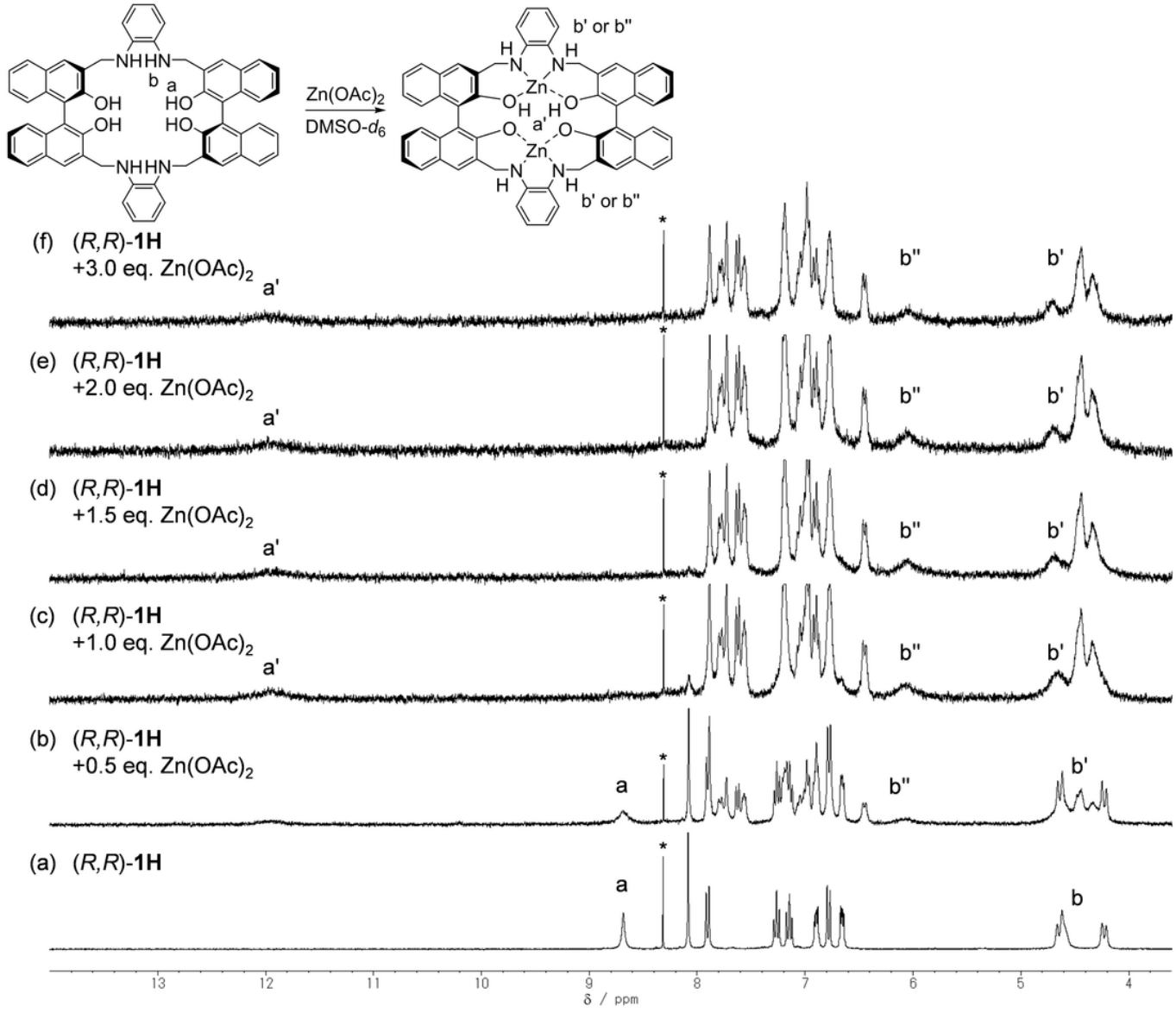

Figure 6

1H NMR spectra of (a) (R,R)-1H; (b) addition of 0.5 equiv of Zn2+; (c) addition of 1.0 equiv of Zn2+; (d) addition of 1.5 equiv of Zn2+; (e) addition of 2.0 equiv of Zn2+; and (f) addition of 3.0 equiv of Zn2+. CHCl3 impurity is labeled by an asterisk.

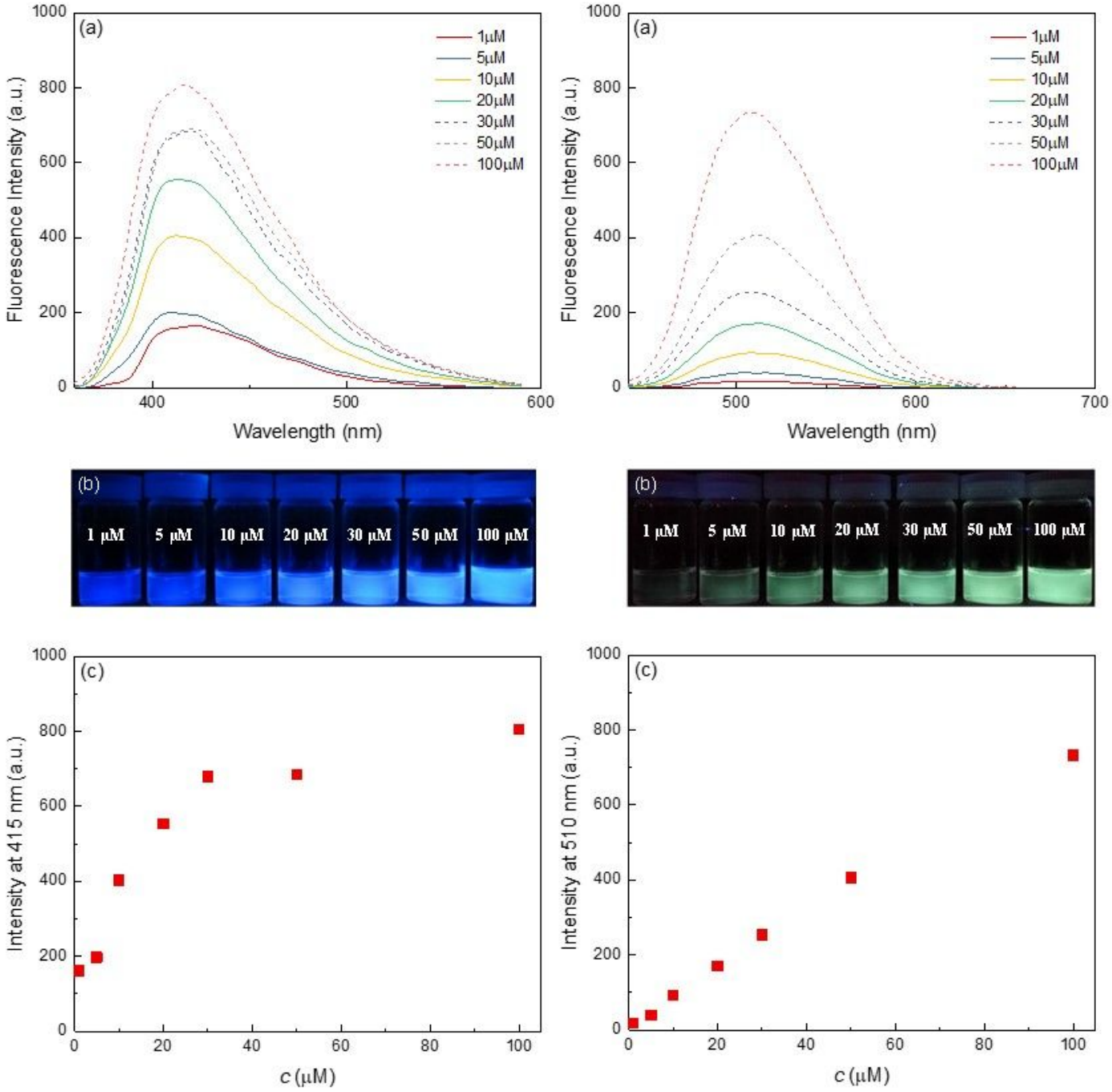

Figure 7

Fluorescence emission spectra (a), photographs under UV lamp (λex =365 nm) (b), and plot of intensity change (c) versus concentration in ethanol (1–100 μM, λex = 340 nm) of (R,R)-2H (left side) and (R,R)-3H (right side) in the presence of Zn2+.

Supplementary Files

This is a list of supplementary files associated with this preprint. Click to download.

- GraphicalAbstract.png
- Scheme1.png
- Chart1.png
- HTMMSI.pdf